



Synthesis and evaluation of novel radioiodinated anthranilate derivatives for in vivo imaging of vascular endothelial growth factor receptor with single-photon emission computed tomography

Masahiko Hirata¹ · Akihiko Asano¹ · Yasuhiro Magata² · Yoshiro Ohmomo^{1,4} · Takashi Temma^{1,3} 

Received: 7 February 2020 / Accepted: 28 April 2020
© The Japanese Society of Nuclear Medicine 2020

Abstract

Objective Angiogenesis facilitates tumor survival and promotes malignancy. The vascular endothelial growth factor (VEGF)/VEGF receptor (VEGFR) tyrosine kinase (TK) signaling pathway is a key factor mediating angiogenesis, suggesting that this pathway may be a target for diagnosis and therapy. In this study, we aimed to develop small molecule radioiodinated probes applicable for in vivo VEGFR imaging considering the versatility and usefulness of single-photon emission computed tomography (SPECT).

Methods We designed and synthesized four radioiodinated anthranilate compounds (**6a–d**) based on the structure of an anticancer drug targeting VEGFR-TK. The inhibitory potencies of corresponding cold compounds **4a–d** and in vitro stability of compounds **6a–d** were assessed by cellular proliferation inhibition assays and radio thin-layer chromatography after incubation in neutral solution. In vivo biodistributions were evaluated by determining radioactivity in tissues of interest after intravenous injection of test compounds in tumor-bearing mice. In vitro and in vivo blocking experiments using a selective VEGFR-TK inhibitor and SPECT/computed tomography (CT) imaging were performed in tumor-bearing mice.

Results The radioiodinated compounds **6a–d** were obtained with more than 68.0% radiochemical yield and more than 95% radiochemical purity. Because compounds **4a–d** showed high inhibitory potencies and compounds **6c** and **6d** showed high in vitro stability, **6c** ($[^{125}\text{I}]m\text{-NPAM}$) and **6d** ($[^{125}\text{I}]p\text{-NPAM}$) were further evaluated. Analysis of the in vivo biodistribution revealed a tumor to blood radioactivity ratio of greater than 4 at 24 h after $[^{125}\text{I}]p\text{-NPAM}$ administration. Accumulation of radioactivity in cultured tumor cells and tumor xenografts after $[^{125}\text{I}]p\text{-NPAM}$ administration was significantly blocked by inhibitor pretreatment. Tumors were clearly imaged at 24 h after $[^{125}\text{I}]p\text{-NPAM}$ injection with SPECT/CT in comparison to that in inhibitor-pretreated tumor-bearing mice.

Conclusion $[^{125}\text{I}]p\text{-NPAM}$ may have potential applications as a lead compound for future development of a clinically usable VEGFR imaging probe for SPECT.

Keywords Vascular endothelial growth factor · Single-photon emission computed tomography · Radioiodine · Angiogenesis · Anthranilate

✉ Yoshiro Ohmomo
ohmomo@gly.oups.ac.jp

✉ Takashi Temma
ttemma@gly.oups.ac.jp

¹ Osaka University of Pharmaceutical Sciences, 4-20-1 Nasahara, Takatsuki, Osaka 569-1094, Japan

² Department of Molecular Imaging, Institute for Medical Photonics Research, Preeminent Medical Photonics

Education and Research Center, Hamamatsu University School of Medicine, 1-20-1 Handayama, Higashi-ku, Hamamatsu 431-3192, Japan

³ Department of Biofunctional Analysis, Osaka University of Pharmaceutical Sciences, 4-20-1 Nasahara, Takatsuki, Osaka 569-1094, Japan

⁴ Education and Research Center for Pharmaceutical Sciences, Osaka University of Pharmaceutical Sciences, 4-20-1 Nasahara, Takatsuki, Osaka 569-1094, Japan

Introduction

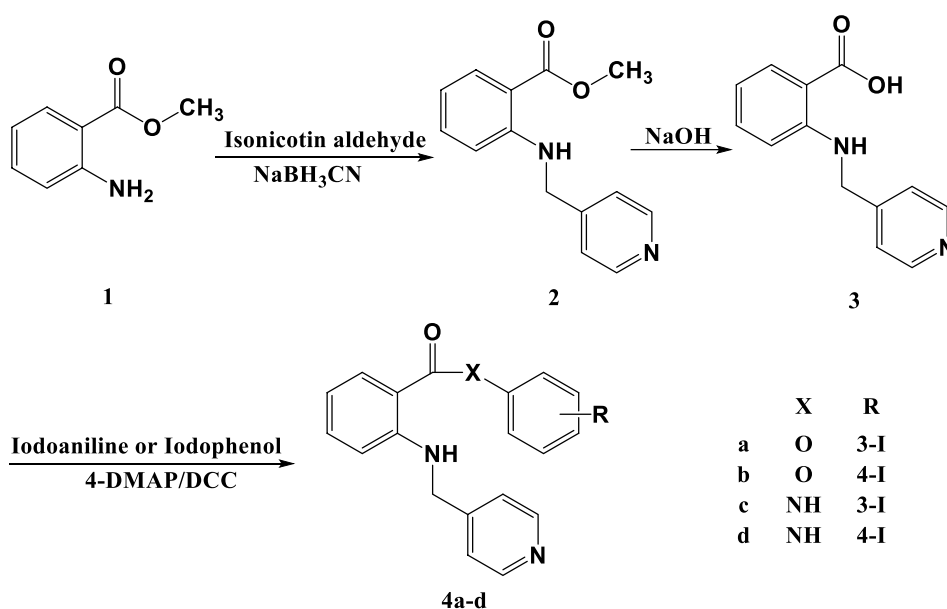
Various receptors are expressed on the surfaces of tumor cells and are related to signaling cascades that control the expression of genes and proteins to regulate tumor characteristics, such as growth, invasion, metastasis, and therapy resistance. Therefore, nuclear medical imaging probes targeting such receptors expressed in tumor cells are essential for elucidation of therapy-related tumor properties.

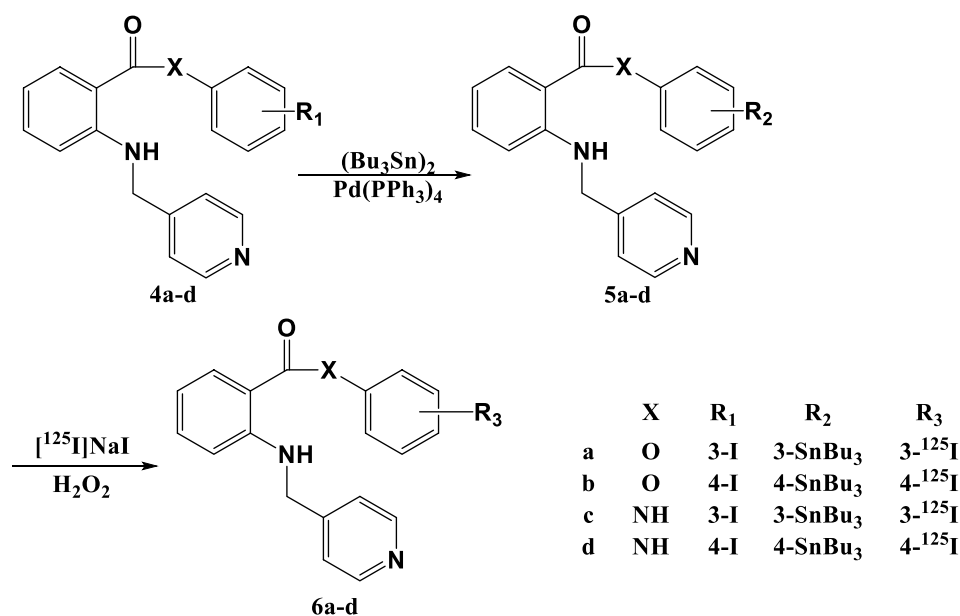
Angiogenesis plays an important role in the efficient supply of nutrients and oxygen to tumors, promoting tumor survival and malignancy. During angiogenesis, the number of abnormal capillary vessels increases; this is a common event that occurs in many malignant tumors and is reportedly related to metastasis and prognosis, suggesting its potential applications as a target for diagnosis and therapy [1–3]. Vascular endothelial growth factor (VEGF) proteins are a family of mitogenic glycoproteins that activate VEGF receptors (VEGFRs) via a tyrosine kinase (TK) signaling pathway. VEGF produced by tumor cells and macrophages is a key player in the angiogenic process in malignant tumors [4–6]. Indeed, therapeutic drugs, such as a humanized anti-VEGF monoclonal antibody (bevacizumab), a Fab fragment of bevacizumab (ranibizumab), and small molecule VEGFR TK inhibitors (sunitinib and sorafenib), have been developed as examples of molecular targeted drugs and are now widely utilized in the clinical setting. Moreover, a variety of imaging probes for positron emission tomography (PET), such as ^{89}Zr -labeled antibody derivatives (^{89}Zr -bevacizumab [7, 8] and ^{89}Zr -ranibizumab [9]), an ^{18}F -labeled sunitinib derivative [10], and ^{18}F - and ^{11}C -labeled sorafenib derivatives [11–13],

have been developed [14], some of which have been evaluated in clinical trials. However, few reports have described the successful development of VEGF imaging probes for single-photon emission computed tomography (SPECT) [15, 16]. Furthermore, to the best of our knowledge, no small molecule imaging probes have been used for in vivo SPECT imaging of VEGF/VEGFR expression to date. Thus, the development of small molecule imaging probes that enable in vivo SPECT imaging of VEGF/VEGFR expression is urgently needed owing to the versatility and usefulness of SPECT.

Anthranilate derivatives have attracted attention owing to their major anticancer effects [17]. Among these compounds, 2-([pyridin-4-ylmethyl]amino)-*N*-(3-[trifluoromethyl]phenyl)benzamide (AAL-993) is an anticancer drug targeting VEGFR-TK [18, 19]. Based on the structure of AAL-993, in this study, we introduced an iodine atom into the benzene ring connected to the anthranilic acid moiety via an ester or amide linker to produce the compounds **4a–d**, as shown in Scheme 1. Since several derivatives having halogen atom (fluorine or chlorine), alkoxy group, or methylthio group on the benzene showed high potencies as such drug candidates in addition to AAL-993 having trifluoromethyl group at *m*-position [17–19], we decided to introduce an iodine atom at *m*- and *p*-positions. Besides, considering the control of stability and blood clearance in vivo recognized as one of important factors of molecular imaging probe, ester and amide linkers were tested. In this study, we first synthesized compounds **4a–d** and radiosynthesized compounds **6a–d**, as shown in Scheme 2, and then performed cellular proliferation inhibition assays and stability estimation in neutral solutions. Subsequently, we further evaluated the potential of selected compounds as VEGFR imaging probes by in vivo

Scheme 1 Synthesis of compounds **4a–d**



Scheme 2 Radiosynthesis of compounds **6a–d**

biodistribution experiments, in vitro and in vivo blocking experiments, and SPECT/CT imaging in tumor-bearing mice.

Materials and methods

Reagents and instruments

The melting points (mp) were determined on a Yanagimoto micro-melting point apparatus MP-500D (Yanaco, Kyoto, Japan) and were uncorrected. The ¹H-nuclear magnetic resonance (NMR) spectra were recorded on a Mercury-300 (Varian, Tokyo, Japan) spectrometer, and the chemical shifts were recorded in δ (ppm) downfield from an internal tetramethylsilane standard. High-resolution mass spectra (HRMS) were measured with JMS-700 [2] (JEOL, Tokyo, Japan) or DIP-181 (JASCO, Tokyo, Japan). The high-performance liquid chromatography (HPLC) system included a 600C pump (Nihon Waters, Tokyo, Japan), a 2487 dual wavelength absorbance detector (Nihon Waters), a 170 NaI radioactivity detector (Beckman Coulter, Tokyo, Japan), and a Cosmosil 5C18-AR column (10×250 mm; Nacalai Tesque, Kyoto, Japan). Radioactivity was measured using an ARC-300 or ARC-380 NaI (Tl) gamma counter (Aloka, Tokyo, Japan). All chemicals used were of reagent grade and were used without purification.

Human umbilical vein endothelial cells (HUVECs) and a medium set for cultivation were obtained from Kurabo Industries (Osaka, Japan). PC-3 cells were provided by the Cell Resource Center for Biomedical Research, Institute of Development, Aging and Cancer, Tohoku University.

Male ddY mice and male BALB/c-nu mice were obtained from Japan SLC (Shizuoka, Japan) and were housed for at least 1 week with free access to food and water before the experiments. The animal experiments in this study were conducted in accordance with the animal experiment guidelines of Osaka University of Pharmaceutical Sciences (approval number, 06025).

Synthesis and radiosynthesis (Schemes 1 and 2)

We synthesized compounds **4a–d** following a previous report [19] with slight modifications.

Methyl 2-([pyridin-4-ylmethyl]amino)benzoate (2)

Methyl anthranilate (**1**) (9.06 g, 60 mmol) and isonicotin aldehyde (10.26 g, 60 mmol) were stirred in distilled methanol (100 ml), followed by addition of acetic acid (3.6 ml) and further stirring for 18 h at room temperature. Sodium cyanotrihydroborate (7.2 g) dissolved in a small amount of methanol was added dropwise to the solution over 2 h and stirred for 2 h. After evaporating the solvent under reduced pressure, ethyl acetate was added to the residue. The solution was washed with saturated sodium bicarbonate and brine and dried over sodium sulfate. After evaporating the solvent, the residue was separated and purified by silica gel column chromatography using ethyl acetate/*n*-hexane (1/1, v/v) as an eluate to obtain **2**: yield, 53.3%; mp, 86.1–86.3 °C.

2-([Pyridin-4-ylmethyl]amino)benzoic acid (3)

Addition of 10% sodium hydroxide to **2** (1.0 g, 4.12 mmol) was followed by reflux for 3 h. After cooling, 20% hydrochloric acid was added to the solution until the pH reached 3–4, with constant stirring on ice. The precipitate was filtered and recrystallized with methanol to obtain **3**: yield, 98.1%; mp, 215.5–215.6 °C; $^1\text{H-NMR}$ (CDCl_3) δ : 4.51 (d,2H), 6.50 (dd,1H), 6.60 (dd,1H), 7.18 (dd,1H), 7.32 (dm,2H), 7.82 (dd,1H), 8.20 (qd,1H), 8.60 (de,2H).

3-Iodophenyl 2-([pyridin-4-ylmethyl]amino)benzoate (4a)

m-Iodophenol (1.21 g, 5.5 mmol) and 4-dimethylaminopyridine (0.672 g, 5 mmol) were mixed in chloroform (50 ml) and stirred for 30 min at room temperature. Compound **3** (1.135 g, 5 mmol) and *N,N'*-dicyclohexylcarbodiimide (1.135 g, 5.5 mmol) were added to the solution and stirred for 24 h at room temperature. After filtering the precipitated impurities, the solvent was evaporated under reduced pressure. The residue was resolved in 1 M hydrochloric acid and extracted with chloroform three times. The organic layer was washed with brine and dried over sodium sulfate. After evaporation and recrystallization with ethanol, silica gel column chromatography using chloroform/methanol (20/1, *v/v*) as an eluate was performed to obtain **4a**: yield, 35.8%; mp, 135.5–135.6 °C; HRMS *m/z* 430.0178, Found 430.0183; $^1\text{H-NMR}$ (CDCl_3) δ : 4.49 (d,2H), 6.55 (d,1H), 6.71 (t,1H), 7.20 (t,1H), 7.25–7.40 (dt,3H + 1H), 7.60 (t,2H), 8.19 (d,2H), 8.65 (d,2H).

4-Iodophenyl 2-([pyridin-4-ylmethyl]amino)benzoate (4b)

Using a method similar to that described above for the synthesis of compound **4a**, *p*-iodophenol (1.21 g, 5.5 mmol) was used instead of *m*-iodophenol to obtain **4b**: yield, 19.5%; mp, 197.1–197.2 °C; HRMS *m/z* 430.0178, Found 430.0180; $^1\text{H-NMR}$ (CDCl_3) δ : 4.52 (d,2H), 6.55 (d,1H), 6.75 (t,1H), 6.98 (d,1H), 7.25–7.40 (st,1H + 3H), 7.76 (d,2H), 8.19 (dd,2H), 8.65 (d,2H).

***N*-(3-Iodophenyl)-2-([pyridin-4-ylmethyl]amino)benzamide (4c)**

Using a method similar to that described above for the synthesis of compound **4a**, *m*-iodoaniline (1.05 g, 4.79 mmol) was used instead of *m*-iodophenol to obtain **4c**: yield, 63.8%; mp, 178.6–178.8 °C; HRMS *m/z* 429.0338, Found

429.0337; $^1\text{H-NMR}$ (CDCl_3) δ : 4.45 (d,2H), 6.55 (d,1H), 6.70 (t,1H), 7.10 (t,1H), 7.25–7.55 (dt,1H + 3H), 7.7 (s,1H), 8.19 (d,2H), 8.65 (d,3H).

***N*-(4-Iodophenyl)-2-([pyridin-4-ylmethyl]amino)benzamide (4d)**

Using a method similar to that described above for the synthesis of compound **4a**, *p*-iodoaniline (1.05 g, 4.79 mmol) was used instead of *m*-iodophenol to obtain **4d**: yield, 31.0%; mp, 70.6–70.8 °C; HRMS *m/z* 429.0338, Found 429.0337; $^1\text{H-NMR}$ (CDCl_3) δ : 4.42 (d,2H), 6.55 (d,1H), 6.73 (t,1H), 7.10 (t,1H), 7.25–7.50 (st,1H + 3H), 7.7 (s,1H), 8.19 (d,2H), 8.65 (d,3H).

Tributylstannyl precursors (5a–d)

After dissolving **4a–d** (0.5 g, 1.16 mmol) in toluene (25 ml), bis(tributyltin) (0.43 ml, 0.85 mmol) and tetrakis(triphenylphosphine) palladium (0.002 g, 0.01 mmol) were added and refluxed for 24 h under argon atmosphere. After cooling to room temperature, the impurities were removed using celite filtration, and the filtrate was evaporated under reduced pressure. The residue was separated and purified by silica gel column chromatography using chloroform/methanol (50/1, *v/v*) as an eluate to obtain **5a–d** as an oily matter.

3-(Tributylstannyl)phenyl 2-([pyridin-4-ylmethyl]amino)benzoate (**5a**): yield, 49.4%; MS-EI *m/z*: 595[M]⁺; $^1\text{H-NMR}$ (CDCl_3) δ : 0.91 (t,9H), 1.18 (t,4H), 1.33 (tt,6H), 1.57 (dt,7H), 4.49 (d,2H), 6.55 (d,1H), 6.73 (t,1H), 7.10 (d,1H), 7.20–7.40 (st,4H + 2H), 8.21 (t,2H), 8.65 (d,2H).

4-(Tributylstannyl)phenyl 2-([pyridin-4-ylmethyl]amino)benzoate (**5b**): yield, 39.7%; MS-EI *m/z*: 595[M]⁺; $^1\text{H-NMR}$ (CDCl_3) δ : 0.91 (t,9H), 1.18 (t,4H), 1.33 (tt,6H), 1.57 (dt,7H), 4.49 (d,2H), 6.55 (d,1H), 6.73 (t,1H), 7.10 (d,1H), 7.20–7.40 (st,4H + 2H), 8.21 (t,2H), 8.65 (d,2H).

2-([Pyridin-4-ylmethyl]amino)-*N*-(3-[tributylstannyl]phenyl)benzamide (**5c**): yield, 29.0%; MS-EI *m/z*: 535[mono desbuthyl fragment]; $^1\text{H-NMR}$ (CDCl_3) δ : 0.91 (t,9H), 1.18 (t,4H), 1.33 (tt,6H), 1.57 (dt,7H), 4.46 (d,2H), 6.51 (d,1H), 6.70 (t,1H), 7.10 (d,1H), 7.20–7.40 (tt,2H + 2H), 7.45 (s,1H), 7.58 (d,1H), 7.68 (d,1H), 7.79 (s,1H), 8.12 (t,1H), 8.54 (d,2H).

2-([Pyridin-4-ylmethyl]amino)-*N*-(4-[tributylstannyl]phenyl)benzamide (**5d**): yield, 24.0%; MS-EI *m/z*: 535[mono desbuthyl fragment]; $^1\text{H-NMR}$ (CDCl_3) δ : 0.91 (t,9H), 1.18 (t,4H), 1.33 (tt,6H), 1.57 (dt,7H), 4.49 (d,2H), 6.55 (d,1H), 6.73 (t,1H), 7.10 (d,1H), 7.20–7.40 (st,4H + 2H), 8.21 (t,2H), 8.65 (d,2H).

Radioiodinated compounds (6a–d)

In a sealed vial, 0.1 M hydrochloric acid solution (25 μ l), [125 I]NaI (3.7–37 MBq/1–10 μ l), and 30 w/v% hydrogen peroxide solution (10 μ l) were sequentially added to precursor tributylstannyl compounds **5a–d** (25 μ l, 1.0 mg/ml methanol solution). The mixture was then allowed to react at room temperature for 15 min. The target radioiodinated compounds **6a–d** were purified by HPLC using methanol/0.01 M phosphate buffer (90/10 or 85/15, v/v) as the mobile phase at a flow rate of 3 ml/min, followed by radiochemical purity analysis. After evaporating the collected HPLC fractions, saline was added to the vial to obtain final formulation for *in vitro* and *in vivo* experiments.

In vitro estimation of inhibitory potencies

HUVECs were cultured in HuMedia-EB2 medium supplemented with 2% fetal calf serum (FCS), human epidermal growth factor, human fibroblast growth factor (basic), hydrocortisone, gentamicin, amphotericin B, and heparin in a CO₂ incubator (5% CO₂ at 37 °C, humidified) in accordance with the manufacturer's instruction. The medium was exchanged every other day and cultured to reach subconfluent conditions for the following experiments. The purities of the compounds **4a–d** used for biological experiments were estimated by HPLC in advance and confirmed to show only single peak detected.

First, HUVECs collected from dishes by trypsin treatment, inoculated at 1.0×10^4 cells/well in 24-well plates, and incubated for 24 h at 37 °C. The medium was exchanged with MCDB131 medium supplemented with 0.5% FCS and further incubated for 24 h. Ten μ l of VEGF (1 μ g/ml) and 100 μ l of 1% dimethyl sulfoxide (DMSO) containing **4a–d** or SU5614 (final concentrations: 1 nM–10 μ M) were added, and samples were incubated for 72 h at 37 °C. The cells were then collected by trypsin treatment, and cell counting was performed to estimate the effects of each tested compound on HUVEC growth. The inhibitory potencies of the compounds were evaluated by determining half-maximal inhibitory concentration (IC₅₀) values taken from inhibition curves plotted as the relationship between the final cell number and the final concentration of each compound added [20].

In vitro stability assay

Compounds **6a–d** (9.25 kBq, 100 μ l), 0.01 M phosphate buffer (pH 7.4, 890 μ l), and 1% bovine serum albumin (10 μ l) were mixed and incubated for 1, 4, and 24 h at 37 °C. At each time point, radioactivity was extracted from the solution with ethyl acetate three times, followed by evaporation under reduced pressure. Normal-phase thin-layer chromatography (TLC) using chloroform/methanol (10/1,

v/v) as an eluent was performed to measure R_f values of the radioactivity to calculate percent intact rates of tested compounds **6a–d** in comparison to R_f values of UV absorbance for control nonradioactive compounds **4a–d**.

Cellular uptake study

PC-3 cells were cultured in RPMI 1640 medium containing 10% FCS supplemented with penicillin–streptomycin solution in a CO₂ incubator (5% CO₂ at 37 °C, humidified) in accordance with the instruction provided by the supplier (IDAC, Tohoku University).

PC-3 cells (1.0×10^5) were suspended in RPMI 1640 medium (serum free, 800 μ l), and 100 μ l of aqueous solution containing 0.05% TritonX and 1% DMSO with or without selective VEGFR-TK inhibitors (VEGFR-TK inhibitor II and SU5614 at a final concentration of 10 μ M) were added to the suspension. Samples were then incubated for 30 min at 37 °C. To the mixed solution, 100 μ l of 10% DMSO containing [125 I]*p*-NPAM (1.85 kBq) was added to a total volume of 1 ml and incubated for 1 h at 37 °C. After the reaction, the solution was suction filtered using a glass filter and washed with 3 ml of 0.2 mM phosphate buffer (pH 7.2). The radioactivity was measured by a gamma counter to estimate diminished rates of cellular uptake of [125 I]*p*-NPAM following inhibitor treatment.

In vivo biodistribution study

A suspension of PC-3 cells (1.0×10^7 cells in 200 μ l RPMI medium containing 10% FCS) was subcutaneously injected into the thighs or the flank of 4-week-old male BALB/c-nu mice (20–25 g). Mice were then raised for 2 weeks. Subsequently, [125 I]*m*-NPAM or [125 I]*p*-NPAM (100 μ l, 18.5 kBq in saline) was injected into tumor-bearing mice via the tail vein. The mice were sacrificed at various time points. Samples of blood and the tissues of interest were excised and weighed. Radioactivity was measured using a gamma counter. Accumulation of radioactivity in each tissue was expressed as a percentage of the injected dose per gram tissue (%ID/g tissue).

To evaluate the specificity of [125 I]*p*-NPAM accumulation in tumors, an *in vivo* pretreatment study was performed. Initially, VEGFR-TK inhibitor II (1.0 mg/kg) or SU5614 (1.0 mg/kg) was intravenously injected into the mice, followed by intravenous injection of [125 I]*p*-NPAM (100 μ l, 18.5 kBq in saline) 5 min later. At 30 min after [125 I]*p*-NPAM administration, the tumors were excised and weighed, and the radioactivity was measured to obtain %ID/g tissue. The data were presented in comparison to the results in the non-pretreated group.

Table 1 Summary of the radiosynthesis of compounds **6a–d**

No	Name	HPLC eluent A/B ^a	Retention time (min)	Radiochemical yield (%)	Radiochemical purity (%)
6a	[¹²⁵ I] <i>m</i> -NPAE	10/90	12.8	90.3	> 95
6b	[¹²⁵ I] <i>p</i> -NPAE	10/90	13.0	97.9	> 95
6c	[¹²⁵ I] <i>m</i> -NPAM	15/85	9.6	95.2	> 95
6d	[¹²⁵ I] <i>p</i> -NPAM	15/85	9.3	68.0	> 95

^aA, 0.01 M phosphate buffer; B, methanol

SPECT/CT

[¹²⁵I]*p*-NPAM (100 μl, 11.1 MBq in saline) was injected into a tumor-bearing mouse via the tail vein. A static SPECT scan acquired over 60 min (60 s × 64 projections, 360°) using a low-energy multi-pinhole collimator (1 mm, energy window; 20–50 keV) was started at 24 h after [¹²⁵I]*p*-NPAM injection using a PET/SPECT/CT FX system (Gamma Medica Ideas, Northridge, CA) [21]. Subsequently, CT images were acquired at 256 projections for 1 min. The mouse was anesthetized under isoflurane during the scans. Following a reconstruction process by OSEM (iteration, 5; subset, 4), the SPECT image was fused with the CT image using Vivid software (Gamma Medica Ideas). A pretreatment study was also performed in a similar way using a tumor-bearing mouse subjected to intravenous injection of SU5614 (1.0 mg/kg) 5 min prior to [¹²⁵I]*p*-NPAM administration.

Statistics

Data are shown as means ± standard deviations. Statistical analyses were performed using Dunnett's multiple comparisons tests as post hoc tests, following one-way analysis of variance. Results with two-tailed *p* values of less than 0.05 were considered statistically significant.

Results and discussion

Synthesis (Scheme 1) and radiosynthesis (Scheme 2)

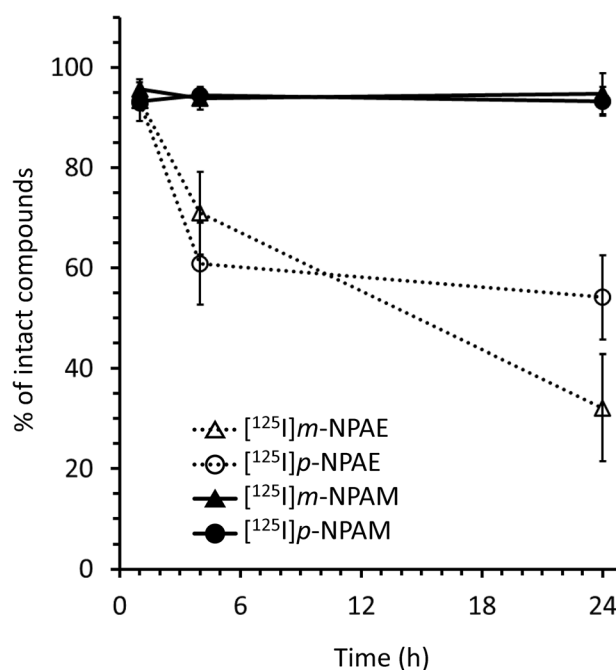
Nonradioactive targeted compounds **4a–d**, which were designed based on the structure of the selective VEGFR-TK inhibitor AAL-993 as a candidate for in vivo SPECT imaging of VEGFR-TK in tumors, were successfully obtained at overall yields of 10.2–33.4% through a three step synthesis, as shown in Scheme 1. The compounds **4a–d** were designated *m*-NPAE, *p*-NPAE, *m*-NPAM, and *p*-NPAM, respectively.

Radioiodinated compounds **6a–d** ([¹²⁵I]*m*-NPAE, [¹²⁵I]*p*-NPAE, [¹²⁵I]*m*-NPAM, and [¹²⁵I]*p*-NPAM) were obtained by an organotin–radioactive iodine exchange

Table 2 Inhibitory potencies (IC₅₀) of compounds **4a–d** in cell proliferation assays

No	Name	IC ₅₀
4a	<i>m</i> -NPAE	61.4 nM
4b	<i>p</i> -NPAE	13.2 nM
4c	<i>m</i> -NPAM	2.53 μM
4d	<i>p</i> -NPAM	12.5 nM
	SU5614	0.44 μM

Each value represents the mean

**Fig. 1** In vitro stability assay. Each value represents the mean ± standard deviation for three samples at each time point

reaction from corresponding tributylstannyl precursors **5a–d**, as shown in Scheme 2. Successful syntheses were confirmed by the coincidence of retention times between UV absorbance peaks of nonradioactive **4a–d** and radioactivity peaks of **6a–d** in chromatograms from reverse-phase HPLC analysis (Table 1). The radiochemical yield and the radiochemical purity of **6a–d** were more than 68.0% and

more than 95%, respectively, as summarized in Table 1. The molar activity of **6a–d** was approximately 81.4 TBq/mmol.

In vitro estimation of inhibitory potency (Table 2) and stability (Fig. 1)

Inhibitory potencies of **4a–d** toward VEGFR-TK activity in HUVECs were measured by cell proliferation assays and compared with the results for SU5614, a representative VEGFR-TK inhibitor (Table 2). As a result, *m*-NPAAE, *p*-NPAAE, *m*-NPAM, and *p*-NPAM showed high inhibitory potencies, with IC_{50} s of 12.5 nM–2.53 μ M, which were comparable to that of SU5614.

Next, to estimate the in vivo availability of the radiiodinated compounds **6a–d**, stability was assessed by normal-phase TLC analysis following incubation for several hours in neutral phosphate buffer. As shown in Fig. 1, [125 I]*m*-NPAM and [125 I]*p*-NPAM stably existed in an intact form in the solution for over 24 h, whereas [125 I]*m*-NPAAE and [125 I]*p*-NPAAE were rapidly degraded. Therefore, on the basis of the above two in vitro experiments, [125 I]*m*-NPAM and [125 I]*p*-NPAM were selected for further evaluation in in vivo experiments owing to their high inhibitory potencies and stabilities.

In vivo biodistribution study (Tables 3 and 4, Fig. 2)

The pharmacokinetics of [125 I]*p*-NPAM and [125 I]*m*-NPAM were evaluated in biodistribution experiments in PC-3 tumor-bearing mice, as shown in Tables 3 and 4, respectively. Notably, [125 I]*p*-NPAM showed high and fast radioactivity accumulation in tumors (2.77%ID/g) at 30 min after

Table 3 Radioactivity biodistribution after intravenous administration of [125 I]*p*-NPAM in tumor-bearing mice

	Time after administration (h)			
	0.5	1	2	24
Blood	1.98 ± 0.20	1.62 ± 0.18	1.27 ± 0.24	0.20 ± 0.01
Pancreas	1.54 ± 0.27	1.14 ± 0.08	0.64 ± 0.12	0.17 ± 0.01
Spleen	1.39 ± 0.08	1.03 ± 0.06	0.66 ± 0.16	0.21 ± 0.04
Stomach	20.48 ± 0.80	12.69 ± 0.71	8.58 ± 0.73	1.17 ± 0.34
Intestine	13.79 ± 1.18	19.61 ± 1.12	23.37 ± 0.95	9.03 ± 0.51
Liver	12.24 ± 1.19	3.93 ± 0.57	2.24 ± 0.34	0.24 ± 0.03
Kidney	3.68 ± 0.29	1.84 ± 0.10	1.07 ± 0.11	0.18 ± 0.01
Heart	1.24 ± 0.18	0.89 ± 0.07	0.45 ± 0.08	0.11 ± 0.02
Lung	3.55 ± 0.50	2.29 ± 0.18	1.20 ± 0.21	0.32 ± 0.09
Brain	0.75 ± 0.13	0.23 ± 0.01	0.09 ± 0.01	0.03 ± 0.01
Tumor	2.77 ± 0.45	1.73 ± 0.14	1.21 ± 0.16	0.85 ± 0.03
Muscle	1.14 ± 0.20	0.71 ± 0.23	0.40 ± 0.05	0.15 ± 0.08

Data are presented as %ID/g tissue. Each value represents the mean ± standard deviation for four animals at each interval

Table 4 Radioactivity biodistribution after intravenous administration of [125 I]*m*-NPAM in tumor-bearing mice

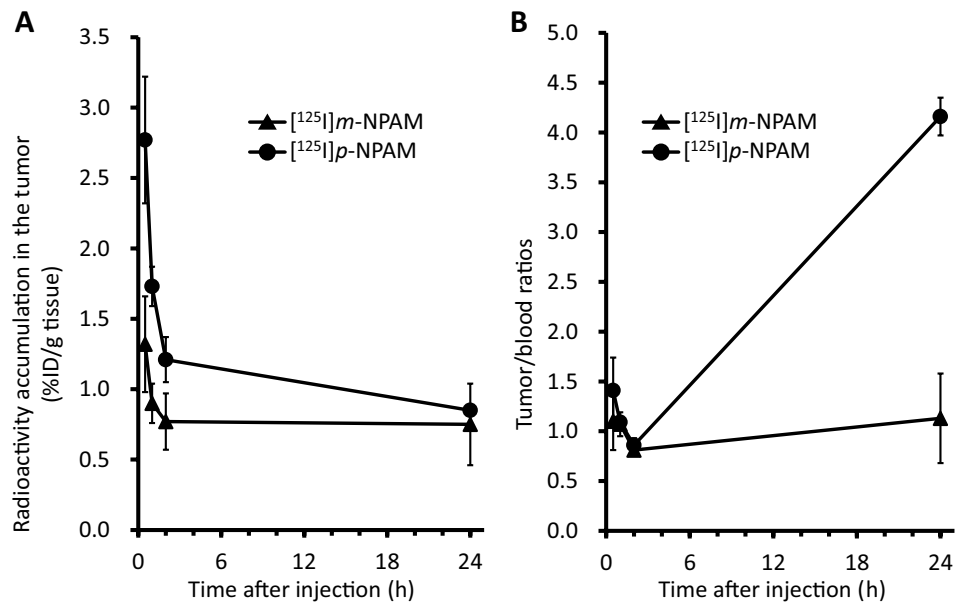
	Time after administration (h)			
	0.5	1	2	24
Blood	1.21 ± 0.11	0.81 ± 0.09	0.83 ± 0.04	0.67 ± 0.06
Pancreas	1.63 ± 0.19	0.77 ± 0.04	0.64 ± 0.03	0.36 ± 0.06
Spleen	0.97 ± 0.13	0.62 ± 0.04	0.50 ± 0.04	0.38 ± 0.05
Stomach	11.47 ± 1.44	11.91 ± 1.49	4.42 ± 0.91	2.89 ± 0.90
Intestine	20.00 ± 1.19	26.12 ± 1.55	30.78 ± 3.12	14.11 ± 1.36
Liver	11.36 ± 1.50	3.50 ± 0.37	2.44 ± 0.99	0.51 ± 0.16
Kidney	4.13 ± 0.38	1.67 ± 0.18	1.21 ± 0.09	0.47 ± 0.07
Heart	1.14 ± 0.14	0.62 ± 0.05	0.44 ± 0.01	0.28 ± 0.02
Lung	2.97 ± 0.40	1.60 ± 0.27	1.40 ± 0.12	0.86 ± 0.22
Brain	0.75 ± 0.05	0.21 ± 0.02	0.11 ± 0.01	0.04 ± 0.01
Tumor	1.32 ± 0.34	0.90 ± 0.14	0.77 ± 0.20	0.75 ± 0.29
Muscle	1.19 ± 0.53	0.44 ± 0.05	0.57 ± 0.24	0.17 ± 0.03

Data are presented as %ID/g tissue. Each value represents the mean ± standard deviation for four animals at each interval

intravenous administration. The tumor radioactivity was then slowly cleared but retained to some extent to give 0.85%ID/g at 24 h (Fig. 2a). The blood radioactivity was the highest at 30 min (1.98%ID/g) and then rapidly cleared to achieve 0.20%ID/g at 24 h. Thus, the radioactivity ratios of tumor/muscle and tumor/blood, important indexes for determining the feasibility of the approach for in vivo imaging, were 2.32 and 1.41, respectively, at 30 min and rose to 5.55 and 4.16, respectively, at 24 h (Fig. 2b). It is previously reported that radiolabeled humanized monoclonal antibody bevacizumab showed high blood radioactivity retention (9.54 and 11.87%ID/g for 89 Zr and 111 In labeled bevacizumab, respectively) and low tumor/blood ratio (0.51 and 0.52 for 89 Zr and 111 In labeled bevacizumab, respectively) at 24 h post-administration in tumor bearing mice [22]. Thus, it is indicated that [125 I]*p*-NPAM succeeded in faster targeting and clearance compared with antibody probes. [125 I]*m*-NPAM also showed the highest tumor radioactivity (1.32%ID/g) at the earliest time point over the experimental period; however, this value was only approximately half that of [125 I]*p*-NPAM (Fig. 2a). The blood radioactivity was not high at 30 min (1.21%ID/g), but slow clearance thereafter retained blood radioactivity as 0.67%ID/g at 24 h. Thus, the tumor/blood radioactivity ratios were 1.10 and 1.13 at 30 min and 24 h (Fig. 2b), respectively, whereas the tumor/muscle radioactivity ratio reached the same range as for [125 I]*p*-NPAM.

Analysis of the excretory routes of [125 I]*p*-NPAM and [125 I]*m*-NPAM from the body indicated that the liver and intestine played important roles owing to high radioactivity accumulation in the liver and intestine in comparison with that in the kidneys (Tables 3 and 4). This was expected based on the high lipophilicity of the compounds (4.2

Fig. 2 Comparison of biodistributions of [125 I] p -NPAM and [125 I] m -NPAM in tumor-bearing mice. a Accumulation of radioactivity in the tumor. b Tumor/blood (T/B) ratio. Each value represents the mean \pm standard deviation for four animals at each interval



clogP value estimated by ChemBioDraw software; PerkinElmer Japan (Tokyo, Japan)). Notably, there was some radioactivity detected in the stomach (Tables 3 and 4), indicating that the deiodination reaction occurred to some extent in vivo; this result was inconsistent with the in vitro stability assay (Fig. 1). Although this was a potential drawback of the study and should be addressed in future studies, we further evaluated the potential of [125 I] p -NPAM in blocking assays and in vivo imaging assays because [125 I] p -NPAM showed superior biodistribution, including high tumor targeting and tumor/blood ratios, in tumor-bearing mice in comparison to [125 I] m -NPAM.

In vitro and in vivo blocking study (Fig. 3)

To estimate the specificity of [125 I] p -NPAM targeting VEGFR-TK expressed in cultured cells and inoculated tumor tissues, blocking experiments were performed using selective VEGFR-TK inhibitors in vitro and in vivo (Fig. 3). The results showed that pretreatment with selective VEGFR-TK inhibitors, such as SU5614 and VEGFR-TK inhibitor II, significantly decreased radioactivity accumulated after [125 I] p -NPAM administration in comparison with those of corresponding control groups both in cultured PC-3 cells (Fig. 3a) and inoculated tumor tissues (Fig. 3b). Therefore, these findings clearly suggested that specific interactions

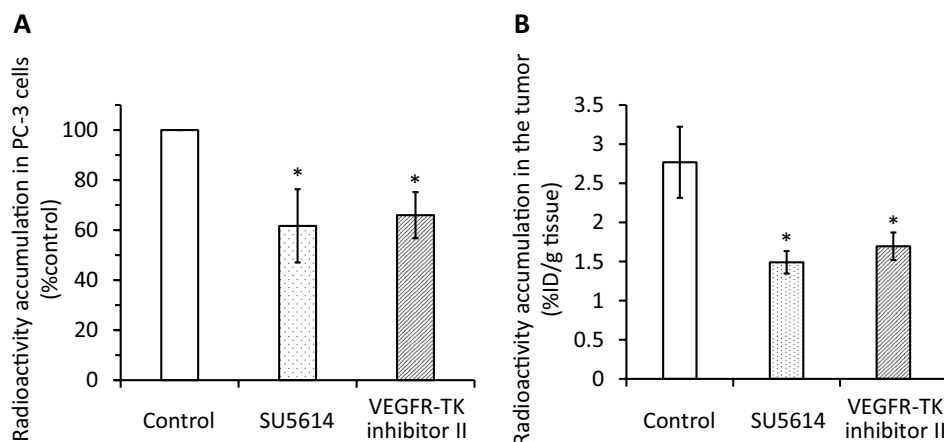


Fig. 3 In vitro and in vivo blocking study. a Radioactivity accumulation (%) in PC-3 cells 1 h after [125 I] p -NPAM addition with or without pretreatment using selective VEGFR-TK inhibitors. Each value represents the mean \pm standard deviation for four samples. b

Radioactivity accumulation (%ID/g tissue) in the tumor 30 min after [125 I] p -NPAM injection with or without pretreatment using selective VEGFR-TK inhibitors. Each value represents the mean \pm standard deviation for 4 animals. * p < 0.05 versus the control

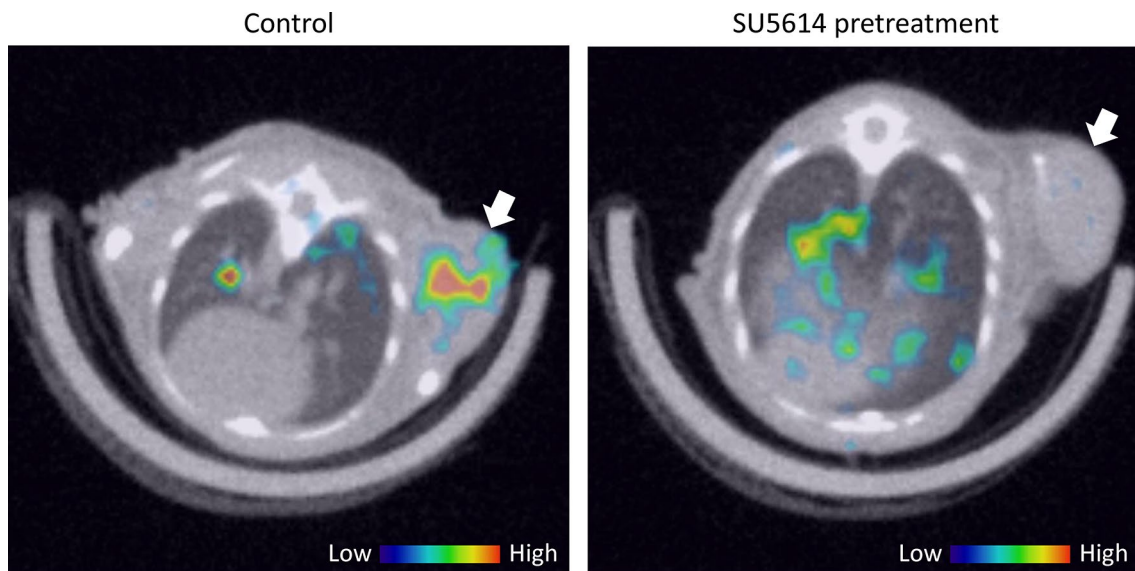


Fig. 4 Fused SPECT/CT images in a transaxial view obtained 24 h after injection of 11.1 MBq [^{125}I]p-NPAM with or without pretreatment using SU5614 in tumor-bearing mice. SPECT and CT scans

between [^{125}I]p-NPAM and VEGFR-TK would significantly contribute to the accumulation of tumor radioactivity after [^{125}I]p-NPAM administration both in vitro and in vivo.

SPECT/CT (Fig. 4)

Lastly, SPECT/CT images were obtained in tumor-bearing mice with a PET/SPECT/CT FX system 24 h after intravenous injection of 11.1 MBq [^{125}I]p-NPAM with or without pretreatment using SU5614 (Fig. 4). The results showed that radioactivity accumulation was observed in the tumor of a control mouse, whereas radioactivity was negligible in the tumor of a pretreated mouse, supporting the findings of the blocking study shown in Fig. 3.

In summary, [^{125}I]p-NPAM, which was designed based on the selective VEGFR-TK inhibitor AAL-993, showed high affinity and stability in vitro and a favorable biodistribution with high radioactivity accumulation in tumors. This compound also exhibited rapid blood clearance, with a tumor to blood radioactivity ratio of 4 at 24 h, enabling in vivo imaging of the tumor tissue in living mice with SPECT. To the best of our knowledge, this is the first report describing the development of a small molecule imaging probe for VEGFR expression in rodent tumors with SPECT. Further refinement of [^{125}I]p-NPAM will encourage the development of superior imaging probes for VEGFR SPECT in a variety of clinical situations. The in vivo instability noted in our biodistribution study could be addressed by further modifications of the chemical structure, and improvement in the pharmacokinetics of [^{125}I]p-NPAM may be necessary to achieve SPECT imaging within several hours after injection by reducing the

were performed over approximately 60 and 1 min, respectively, under isoflurane anesthesia. The white arrows indicate tumor site

lipophilicity of the probe. Accordingly, such refinement of [^{125}I]p-NPAM may lead to the development of promising VEGFR imaging probes for use with SPECT in the future. Among the four anthranilate derivatives synthesized in this study, [^{125}I]p-NPAM may have potential applications as a lead compound for future refinement of in vivo VEGFR imaging with SPECT.

Acknowledgements The authors have no competing interests to declare. This work was partly supported by JSPS KAKENHI (Grant nos. 19591437 and 19H03606). The funding bodies had no role in study design, data collection and analysis, decision to publish, or manuscript preparation.

References

1. Folkman J. Tumor angiogenesis: therapeutic implications. *N Engl J Med.* 1971;285(21):1182–6.
2. Leenders WP, Kusters B, de Waal RM. Vessel co-option: how tumors obtain blood supply in the absence of sprouting angiogenesis. *Endothelium.* 2002;9(2):83–7.
3. Terry SY, Rijpkema M, Abiraj K, van der Graaf WT, Oyen WJ, Boerman OC. Radiolabeled imaging probes targeting angiogenesis for personalized medicine. *Curr Pharm Des.* 2014;20(14):2293–307.
4. Ferrara N. Vascular endothelial growth factor: basic science and clinical progress. *Endocr Rev.* 2004;25(4):581–611.
5. Goldman CK, Kendall RL, Cabrera G, Soroceanu L, Heike Y, Gillespie GY, et al. Paracrine expression of a native soluble vascular endothelial growth factor receptor inhibits tumor growth, metastasis, and mortality rate. *Proc Natl Acad Sci USA.* 1998;95(15):8795–800.
6. Prewett M, Huber J, Li Y, Santiago A, O'Connor W, King K, et al. Antivascular endothelial growth factor receptor (fetal liver

- kinase 1) monoclonal antibody inhibits tumor angiogenesis and growth of several mouse and human tumors. *Cancer Res.* 1999;59(20):5209–18.
7. Gaykema SB, Brouwers AH, Lub-de Hooge MN, Pleijhuis RG, Timmer-Bosscha H, Pot L, et al. ^{89}Zr -bevacizumab PET imaging in primary breast cancer. *J Nucl Med.* 2013;54(7):1014–8.
 8. van Es SC, Brouwers AH, Mahesh SVK, Leliveld-Kors AM, de Jong IJ, Lub-de Hooge MN, et al. ^{89}Zr -Bevacizumab PET: potential early indicator of everolimus efficacy in patients with metastatic renal cell carcinoma. *J Nucl Med.* 2017;58(6):905–10.
 9. Chopra A. ^{89}Zr -Labeled N-succinyl-desferrioxamine-ranibizumab. *Molecular Imaging and Contrast Agent Database (MICAD)*. Bethesda: National Center for Biotechnology Information (US); 2004.
 10. Wang JQ, Miller KD, Sledge GW, Zheng QH. Synthesis of [^{18}F]SU11248, a new potential PET tracer for imaging cancer tyrosine kinase. *Bioorg Med Chem Lett.* 2005;15(19):4380–4.
 11. Asakawa C, Ogawa M, Kumata K, Fujinaga M, Kato K, Yamasaki T, et al. [^{11}C]sorafenib: radiosynthesis and preliminary PET study of brain uptake in P-gp/Bcrp knockout mice. *Bioorg Med Chem Lett.* 2011;21(8):2220–3.
 12. Ilovich O, Åberg O, Långström B, Mishani E. Rhodium-mediated [^{11}C]carbonylation: a library of *N*-phenyl-*N'*-(4-(4-quinolyloxy)phenyl)-[^{11}C]urea derivatives as potential PET angiogenic probes. *J Label Compd Radiopharm.* 2009;52(5):151–7.
 13. Ilovich O, Jacobson O, Aviv Y, Litchi A, Chisin R, Mishani E. Formation of fluorine-18 labeled diaryl ureas-labeled VEGFR-2/PDGFR dual inhibitors as molecular imaging agents for angiogenesis. *Bioorg Med Chem.* 2008;16(8):4242–51.
 14. Kniess T. Radiolabeled small molecule inhibitors of VEGFR - recent advances. *Curr Pharm Des.* 2012;18(20):2867–74.
 15. Kuchar M, Oliveira MC, Gano L, Santos I, Kniess T. Radioiodinated sunitinib as a potential radiotracer for imaging angiogenesis-radiosynthesis and first radiopharmacological evaluation of 5-[^{125}I]Iodo-sunitinib. *Bioorg Med Chem Lett.* 2012;22(8):2850–5.
 16. Rainer E, Wang H, Traub-Weidinger T, Widhalm G, Fueger B, Chang J, et al. The prognostic value of [^{123}I]-vascular endothelial growth factor ([^{123}I]-VEGF) in glioma. *Eur J Nucl Med Mol Imaging.* 2018;45(13):2396–403.
 17. Cocco MT, Congiu C, Lilliu V, Onnis V. Synthesis of new *N*-(2-(trifluoromethyl)pyridin-4-yl)anthranilic acid derivatives and their evaluation as anticancer agents. *Bioorg Med Chem Lett.* 2004;14(23):5787–91.
 18. Furet P, Bold G, Hofmann F, Manley P, Meyer T, Altmann K-H. Identification of a new chemical class of potent angiogenesis inhibitors based on conformational considerations and database searching. *Bioorg Med Chem Lett.* 2003;13(18):2967–71.
 19. Manley PW, Furet P, Bold G, Brügger J, Mestan J, Meyer T, et al. Anthranilic acid amides: a novel class of antiangiogenic VEGF receptor kinase inhibitors. *J Med Chem.* 2002;45(26):5687–93.
 20. Xin X, Yang S, Kowalski J, Gerritsen ME. Peroxisome proliferator-activated receptor gamma ligands are potent inhibitors of angiogenesis in vitro and in vivo. *J Biol Chem.* 1999;274(13):9116–211.
 21. Sakai T, Saito Y, Takashima M, Ogawa M, Magata Y. Development of radioiodinated lipophilic cationic compounds for myocardial imaging. *Nucl Med Biol.* 2015;42(5):482–7.
 22. Nagengast WB, de Vries EG, Hospers GA, Mulder NH, de Jong JR, Hollema H, et al. In vivo VEGF imaging with radiolabeled bevacizumab in a human ovarian tumor xenograft. *J Nucl Med.* 2007;48(8):1313–9.

Publisher's Note Springer Nature remains neutral with regard to jurisdictional claims in published maps and institutional affiliations.